Electronic Supplementary Material (ESI) for Journal of Materials Chemistry C.

Strain-driven topological quantum phase transition in (pseudo)-cubic (mixed)-Cs/MA/FA halide perovskites†

Ankita Phutela,* Sajjan Sheoran, Deepika Gill, and Saswata Bhattacharya*

Department of Physics, Indian Institute of Technology Delhi, New Delhi, India

E-mail: Ankita@physics.iitd.ac.in[AP]; saswata@physics.iitd.ac.in[SB]

Phone: +91-11-2659 1359. Fax: +91-11-2658 2037

Supplementary Information

I. Relaxed structures of cubic and pseudocubic $FAPbI_3$ and partial density of states of $FAPbI_3$.

II. Band profile of $FAPbI_3$ using PBE+SOC and G_0W_0@HSE06+SOC and band inversion using HSE06+SOC ϵ_{xc} functionals.

III. Structural stability of cubic $FAPbI_3$, pseudocubic $FAPbI_3$ and mixed cation perovskites viz. $Cs_{0.5}MA_{0.5}PbI_3$, $Cs_{0.75}MA_{0.25}PbI_3$ and $Cs_{0.25}MA_{0.75}PbI_3$.

IV. Tight-Binding Model.

V. TB bands fitted with DFT bands.

VI. Surface states of $FAPbI_3$ in a different configuration and probability of occurance of different configurations of $FAPbI_3$.

VII. Continuous TPT in cubic $CsPbI_3$.

VIII. TPT in cubic and pseudocubic $MAPbI_3$.

IX. Crystal structures of $Cs_{0.5}MA_{0.5}PbI_3$, $Cs_{0.75}MA_{0.25}PbI_3$ and $Cs_{0.25}MA_{0.75}PbI_3$.

X. TB parameters for $Cs_{0.5}MA_{0.5}PbI_3$.

Relaxed structures of cubic and pseudocubic $FAPbI_3$ and partial density of states of $FAPbI_3$.

C1N2H5Pb1I3-cubic

1.0

6.3631000 0.0000000 0.0000000

0.0000000 6.3631000 0.0000000

0.0000000 0.0000000 6.3631000

H C N I Pb

5 1 2 3 1

Direct

0.500000 0.575336 0.500000

0.683424 0.481765 0.500000

0.316573 0.481765 0.500000

0.500000 0.746958 0.500000

0.813572 0.574741 0.500000

0.704200 0.322745 0.500000

0.295799 0.322745 0.500000

0.186427 0.574741 0.500000

0.000000 0.988000 0.000000

0.500000 0.992253 0.000000

0.000000 0.487339 0.000000

0.000000 0.978411 0.500000

C1N2H5Pb1I3-pseudocubic

1.0

6.3631000 0.0000000 0.0000000

0.0000000 6.3631000 0.0000000

0.0000000 0.0000000 6.3631000

H C N I Pb

5 1 2 3 1

Direct

0.497310 0.746640 0.493147

0.501923 0.565693 0.184682

0.503670 0.316979 0.301112

0.500074 0.328511 0.709218

0.496402 0.583402 0.811370

0.499156 0.575147 0.498009

0.501777 0.476467 0.317372

0.498547 0.486826 0.683958

0.004816 0.497332 0.069536

0.068890 -0.069536 0.492561

0.497421 0.004816 -0.068890

0.000000 0.000000 0.000000

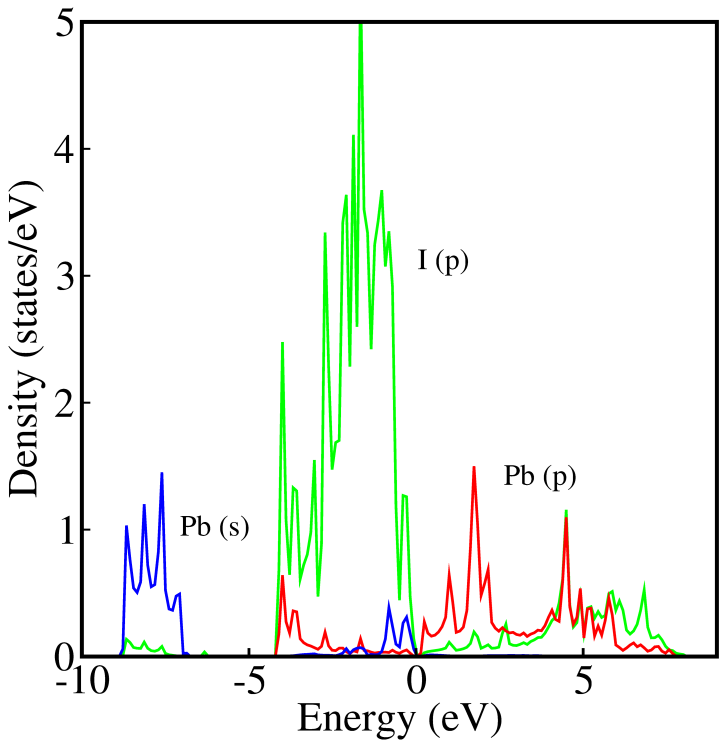

Figure S1: Partial denisty of states for $FAPbI_3$ showing I-p, Pb-s and Pb-p states in green, blue and red colours, respectively.

Band profile of $FAPbI_3$ using PBE+SOC and G_0W_0@HSE06+SOC and band inversion using HSE06+SOC ϵ_{xc} functionals.

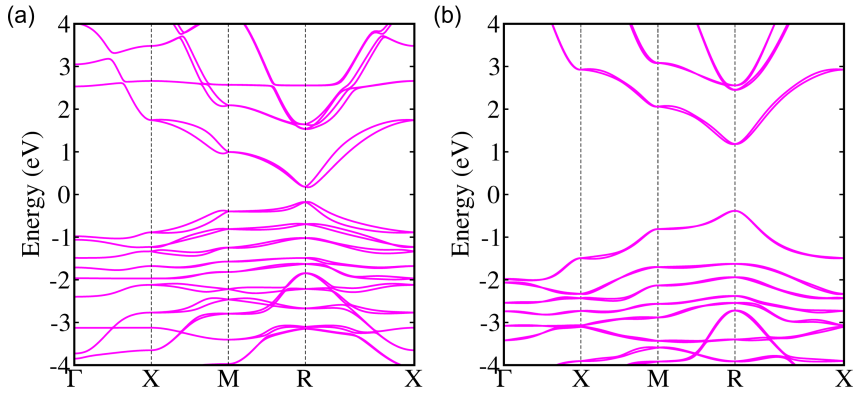

Figure S2: Band structure of $FAPbI_3$ calculated using (a) PBE+SOC and (b) G_0W_0@HSE06+SOC.

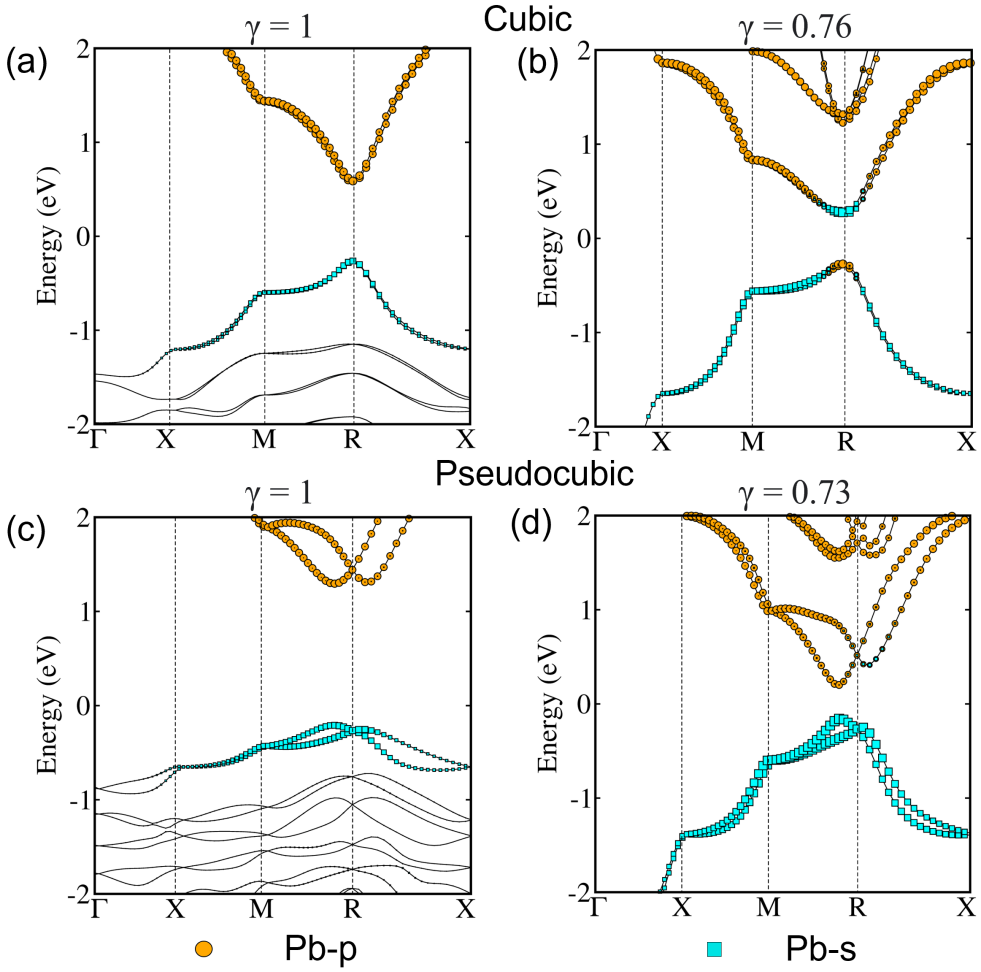

Figure S3: Orbital resolved HSE06+SOC band structure for cubic and pseudocubic $FAPbI_3$ (a), (d) without compression, and (b), (e) at critical compression $\gamma = 0.76$, and $\gamma = 0.73$, respectively.

Structural stability of cubic $FAPbI_3$, pseudocubic $FAPbI_3$ and mixed cation perovskites viz. $Cs_{0.5}MA_{0.5}PbI_3$, $Cs_{0.75}MA_{0.25}PbI_3$ and $Cs_{0.25}MA_{0.75}PbI_3$.

We have checked the structural stability of cubic and pseudocubic $FAPbI_3$ along with the strained configurations using ab *initio* molecular dynamics (AIMD). For this, we have obtained the radial distribution function (g(r)) at T = 0 K and T = 300 K. We have observed that the nature of radial distribution function remains the same at room temperature for the nearest neighbors (see Figure S4). Therefore, we validate that the configurations are structurally stable at 300 K even after undergoing compression. This makes them useful in realizing the practical applications.

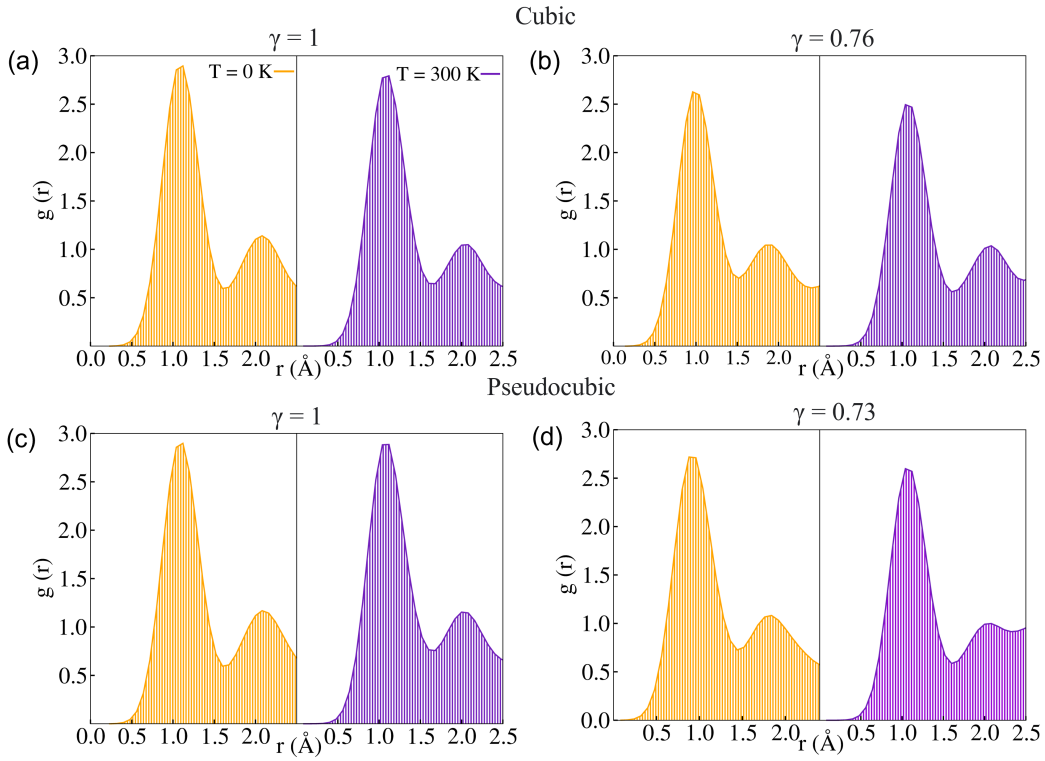

Figure S4: Radial distribution function using NVT ensemble for different phases of $FAPbI_3$ namely (a) cubic, (b) strained cubic ($\gamma = 0.76$), (c) pseudocubic and (d) strained pseudocubic ($\gamma = 0.73$) at T = 0 K and T = 300 K.

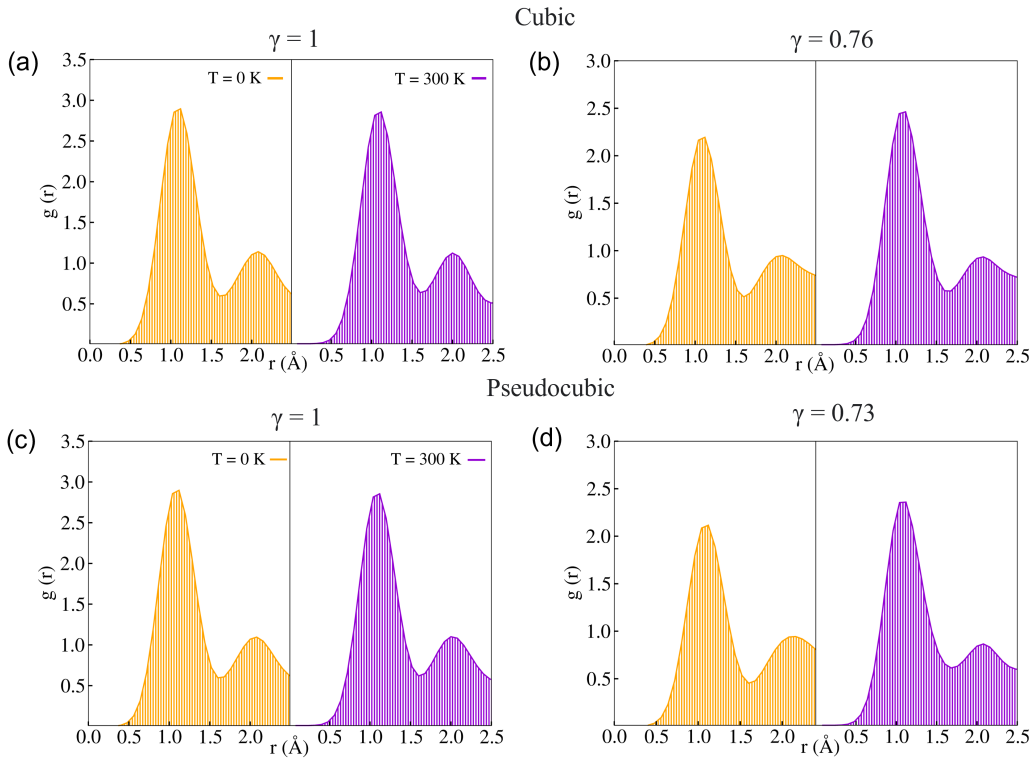

Figure S5: Radial distribution function using NPT ensemble for different phases of $FAPbI_3$ namely (a) cubic, (b) strained cubic ($\gamma = 0.76$), (c) pseudocubic and (d) strained pseudocubic ($\gamma = 0.73$) at T = 0 K and T = 300 K.

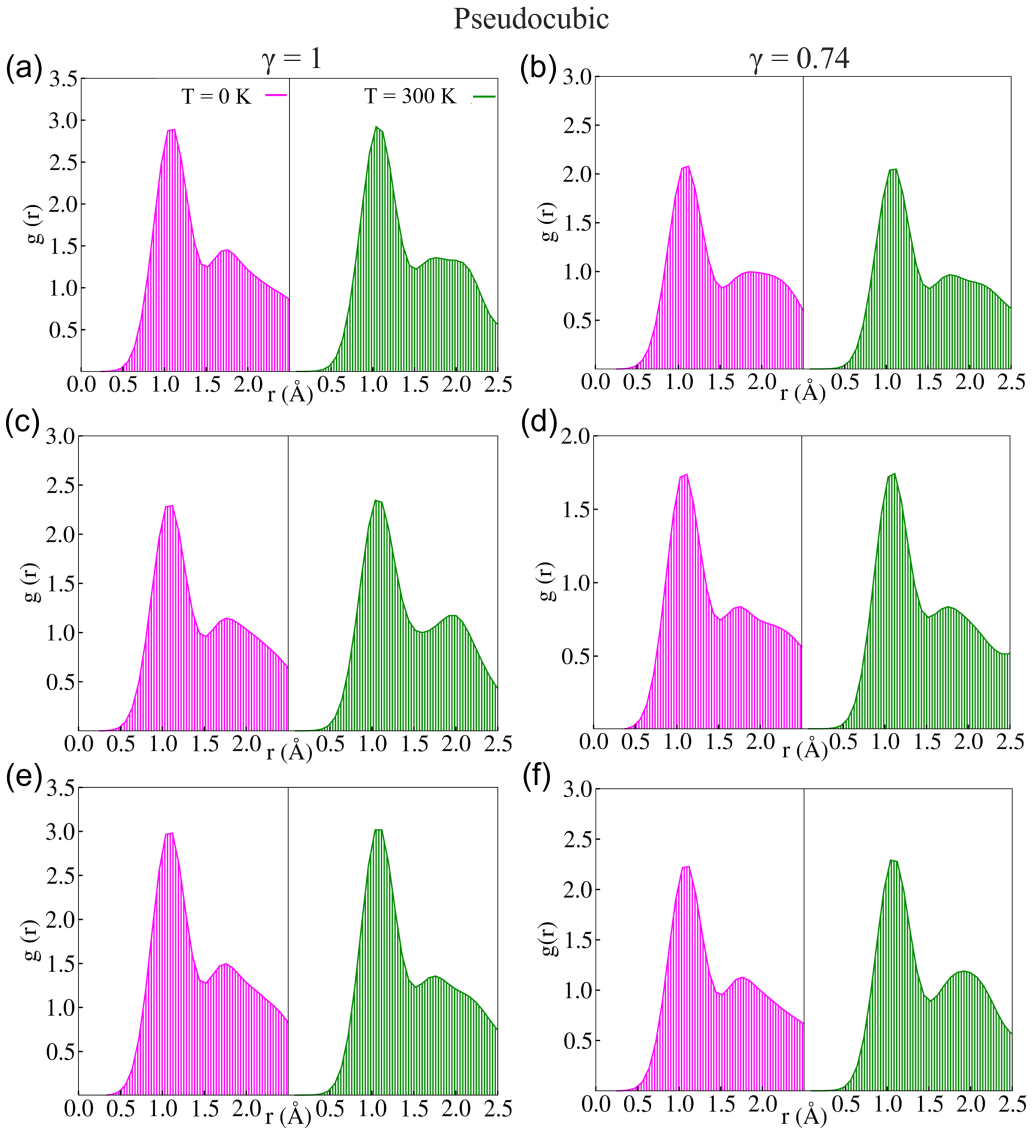

Figure S6: Radial distribution function at T = 0 K and T = 300 K for unstrained and strained ($\gamma = 0.74$), (a), (b) $Cs_{0.5}MA_{0.5}PbI_3$, (c), (d) $Cs_{0.75}MA_{0.25}PbI_3$, (e) and (f) $Cs_{0.25}MA_{0.75}PbI_3$, respectively.

Tight-Binding Model.

The individual blocks of the matrix are as follows

$$M_{4\times4}^{Pb-Pb}=\begin{pmatrix}\epsilon_s+g_1 & 2it_{sp\sigma}^{Pb-Pb}Sin(k_xa) & 2it_{sp\sigma}^{Pb-Pb}Sin(k_ya) & 2it_{sp\sigma}^{Pb-Pb}Sin(k_za)\\ -2it_{sp\sigma}^{Pb-Pb}Sin(k_ya) & \epsilon_{p1}+g_2 & 0 & 0\\ -2it_{sp\sigma}^{Pb-Pb}Sin(k_xa) & 0 & \epsilon_{p1}+g_3 & 0\\ -2it_{sp\sigma}^{Pb-Pb}Sin(k_za) & 0 & 0 & \epsilon_{p1}+g_4\end{pmatrix} \tag{1}$$

$$M_{4\times9}^{Pb-I}=\begin{pmatrix}t_{sp\sigma}^{Pb-I}S_x & 0 & 0 & 0 & t_{sp\sigma}^{Pb-I}S_y & 0 & 0 & 0 & t_{sp\sigma}^{Pb-I}S_z\\ t_{pp\sigma}^{Pb-I}C_x & 0 & 0 & t_{pp\pi}^{Pb-I}C_y & 0 & 0 & t_{pp\pi}^{Pb-I}C_z & 0 & 0\\ 0 & t_{pp\pi}^{Pb-I}C_x & 0 & 0 & t_{pp\pi}^{Pb-I}C_y & 0 & 0 & t_{pp\pi}^{Pb-I}C_z & 0\\ 0 & 0 & t_{pp\pi}^{Pb-I}C_x & 0 & 0 & t_{pp\pi}^{Pb-I}C_y & 0 & 0 & t_{pp\sigma}^{Pb-I}C_z\end{pmatrix} \tag{2}$$

$$M_{9\times9}^{I-I}=\begin{pmatrix}\epsilon_{p2} & 0 & 0 & 0 & 0 & 0 & 0 & 0 & 0\\ 0 & \epsilon_{p2} & 0 & 0 & 0 & 0 & 0 & 0 & 0\\ 0 & 0 & \epsilon_{p2} & 0 & 0 & 0 & 0 & 0 & 0\\ 0 & 0 & 0 & \epsilon_{p2} & 0 & 0 & 0 & 0 & 0\\ 0 & 0 & 0 & 0 & \epsilon_{p2} & 0 & 0 & 0 & 0\\ 0 & 0 & 0 & 0 & 0 & \epsilon_{p2} & 0 & 0 & 0\\ 0 & 0 & 0 & 0 & 0 & 0 & \epsilon_{p2} & 0 & 0\\ 0 & 0 & 0 & 0 & 0 & 0 & 0 & \epsilon_{p2} & 0\\ 0 & 0 & 0 & 0 & 0 & 0 & 0 & 0 & \epsilon_{p2}\end{pmatrix}. \tag{3}$$

Here ϵ_s ,ϵ_{p1} , and ϵ_{p2} are the onsite energies of Pb-s, Pb-p and I-p orbitals, respectively. The terms C_z and S_z are the representations for $2\cos(k_za/2)$ and $2i\sin(k_za/2)$, and g_i (i = 1,2,3,4) are the $\boldsymbol{k}$-dependent hopping integrals arising from the Pb-Pb second neighbor interactions

given by

$$
\begin{aligned}
g_1 &= 2t_{ss}^{Pb-Pb}[\cos(k_x a) + \cos(k_y a) + \cos(k_z a)], \\
g_2 &= 2t_{pp\sigma}^{Pb-Pb}\cos(k_x a) + 2t_{pp\pi}^{Pb-Pb}[\cos(k_y a) + \cos(k_z a)], \\
g_3 &= 2t_{pp\sigma}^{Pb-Pb}\cos(k_y a) + 2t_{pp\pi}^{Pb-Pb}[\cos(k_x a) + \cos(k_z a)], \\
g_4 &= 2t_{pp\sigma}^{Pb-Pb}\cos(k_z a) + 2t_{pp\pi}^{Pb-Pb}[\cos(k_x a) + \cos(k_y a)].
\end{aligned}
\tag{4}
$$

TB bands fitted with DFT bands.

The TB Hamiltonian is diagonalized and the resulted bands are fitted with that of DFT. The TB bands are plotted in brown while DFT bands are in blue. We find an excellent agreement between the TB and DFT bands (see FIG. S7).

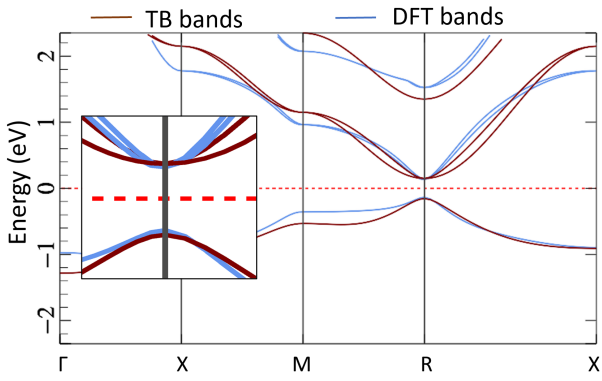

Figure S7: TB bands (brown) fitted with DFT bands (blue).

Surface states of $FAPbI_3$ in a different configuration and probability of occurance of different configurations of $FAPbI_3$.

We have studied the effect on strain on two different orientations of FA i.e., n = 2 and n = 4 (see Figure S9 for n = 2, 4). In both the orientations FA is perpendicular to each other and both show topological phase transition at the critical value of strain (see Figure S8). For MA a different orientation has already been studied in ref.[1]

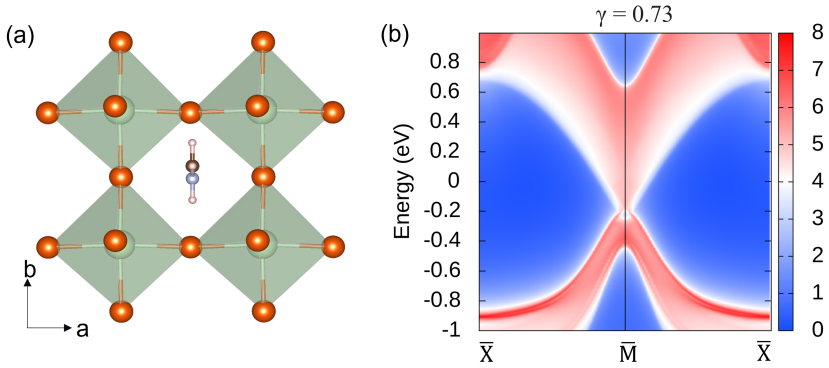

Figure S8: (a) Crystal structure of $FAPbI_3$ showing a different orientation of FA cation and (b) topological surface states at critical strain value.

However, many different orientations of these organic molecules are indeed possible. Therefore, in order to ensure the validity of our above analysis, we have estimated the probability of occurance of different possible pseudocubic congfigurations at T=300 K. Here, we assume that a total of N different configurations are possible out of which N_n is the number of a given type (here n = 4) and its probability of occurrence is given as per Fermi-Dirac statistics as follows [see theoretical derivations in [2,3]]:

$$\frac{N_n}{N} = \frac{exp(-\beta \Delta G_n)}{1 + \sum_m exp(-\beta \Delta G_m)} \tag{5}$$

Here, $\frac{N_n}{N}$ is the probablity of occurance and ΔG is the Gibbs free energy of formation of the type-n configuration. As the range of $\frac{N_n}{N} \times 100$ is significantly large, we have taken the logarithm of the above equation (see Figure S9). The maximum possible value of y-axis is

$\sim$2, when N_n = N, i.e., type-n is the most dominant configuration. Here, we can see that the concentration of different configurations are comparable.

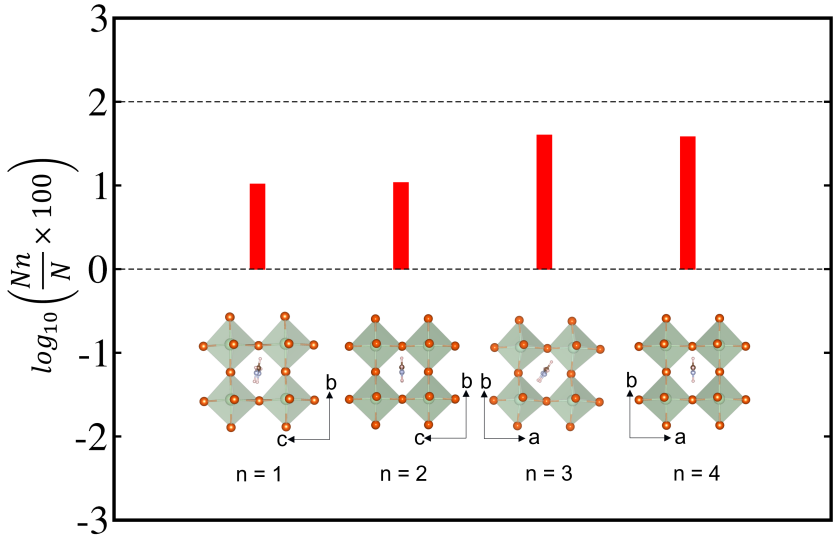

Figure S9: Logarithm of probability of occurance of different configurations at T = 300 K. Orientation of FA is different in all the configurations.

Continous TPT in cubic $CsPbI_3$.

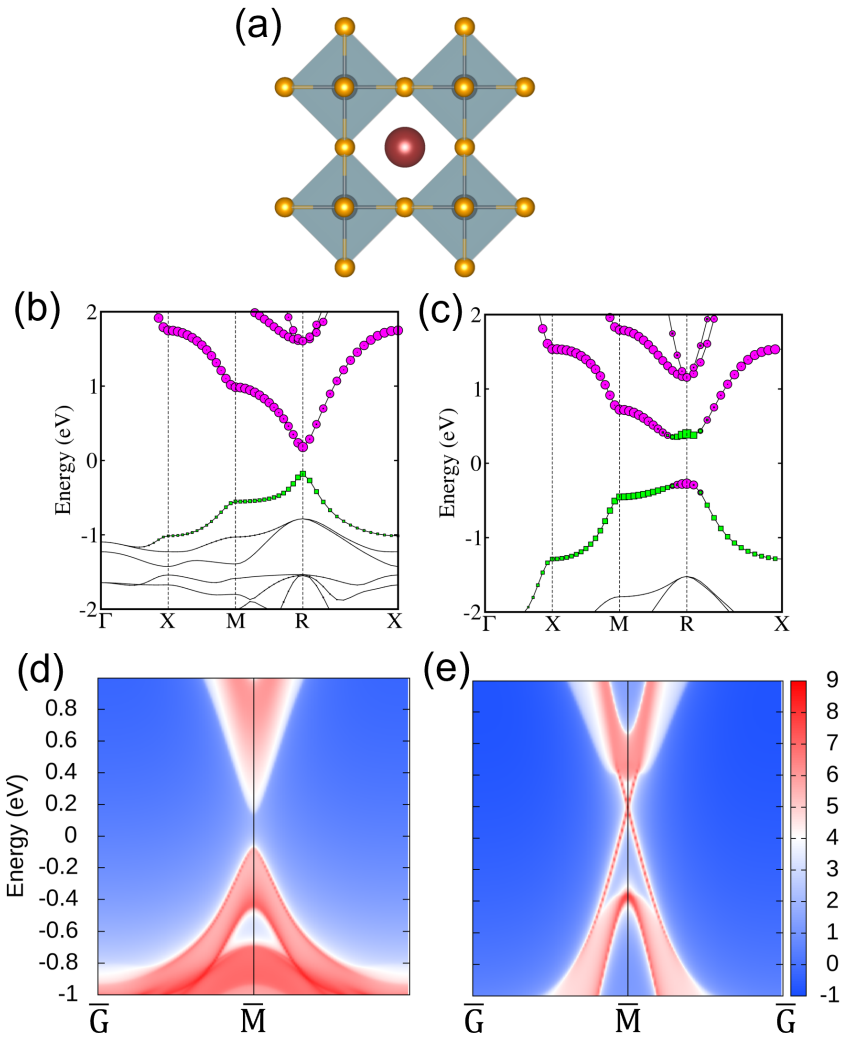

Figure S10: (a) Crystal structure of cubic $CsPbI_3$. Bulk band structure (b) without compression with Pb-p (magenta) contribution at CBM and Pb-s (green) contribution at VBM, and (c) with compression γ= 0.76, showing band inversion at R point. Surface band structure (d) without, and (e) with compression, showing a continuous tranistion from normal to topological state.

TPT in cubic and pseudocubic $MAPbI_3$.

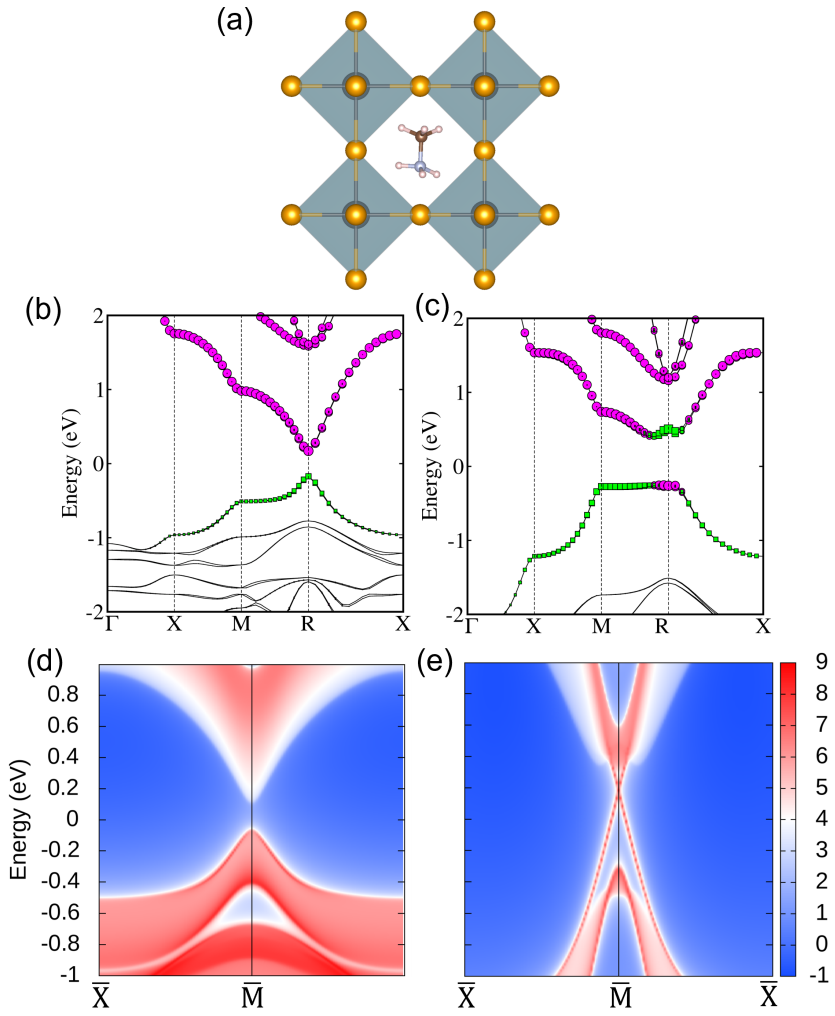

Figure S11: (a) Crystal structure of cubic $MAPbI_3$. Bulk band structure (b) without compression with Pb-p (magenta) contribution at CBM and Pb-s (green) contribution at VBM, and (c) with compression γ= 0.73, showing band inversion at R point. Surface band structure (d) without, and (e) with compression γ= 0.73, showing a continuous tranistion from normal to topological state.

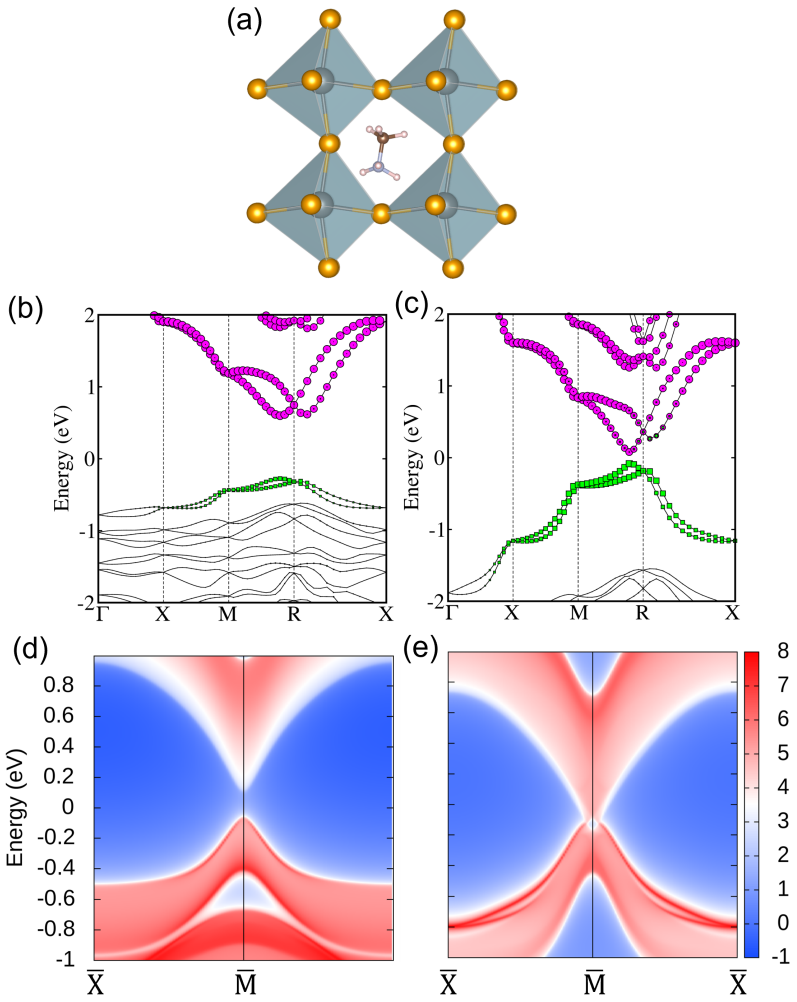

Figure S12: (a) Crystal structure of pseudocubic $MAPbI_3$. Bulk band structure (b) without compression with Pb-p contribution at CBM and Pb-s contribution at VBM, and (c) with compression γ= 0.73, showing band inversion at R point. Surface band structure (d) without, and (e) with compression γ= 0.73, showing a discontinuous tranistion from normal to topological state.

Crystal structures of $Cs_{0.5}MA_{0.5}PbI_3$, $Cs_{0.75}MA_{0.25}PbI_3$ and $Cs_{0.25}MA_{0.75}PbI_3$.

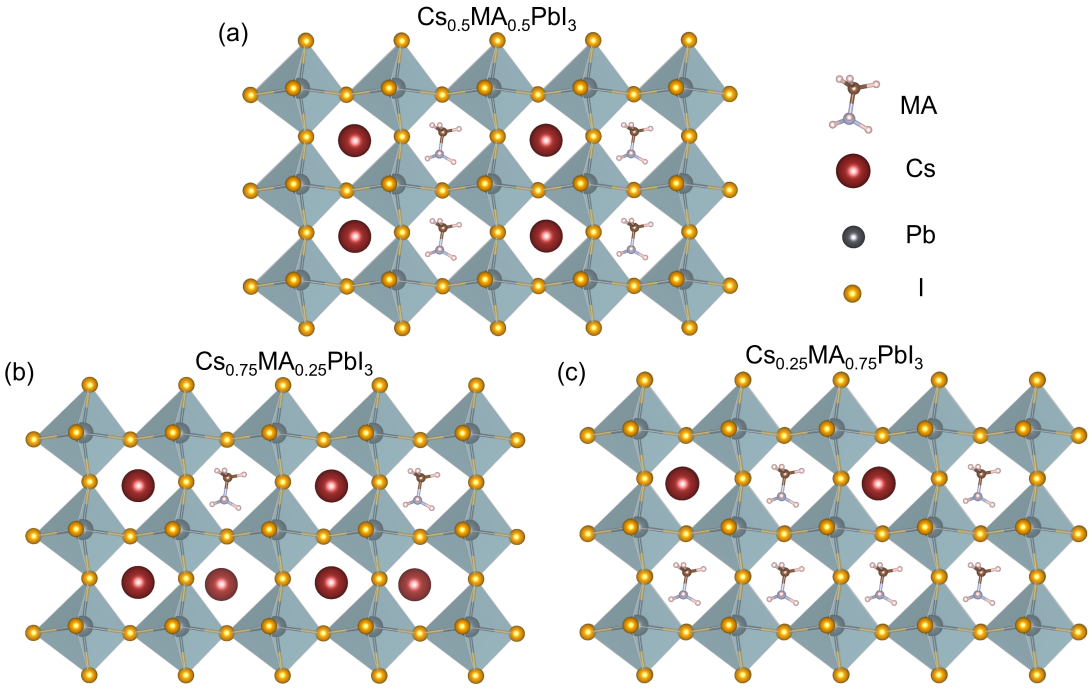

Figure S13: Crytsal structure of (a) $Cs_{0.75}MA_{0.5}PbI_3$, (b) $Cs_{0.5}MA_{0.5}PbI_3$ and (c) $Cs_{0.25}MA_{0.75}PbI_3$.

TB parameters for $Cs_{0.5}MA_{0.5}PbI_3$.

Table S1: Interaction parameters and SOC strength for $Cs_{0.5}MA_{0.5}PbI_3$ from thirteen band hamiltonian at zero and critical compression strength in units of eV.

Type	E_{Pb-s}	E_{Pb-p}	E_{I-p}	$t_{sp\sigma}^{Pb-I}$	$t_{pp\sigma}^{Pb-I}$	$t_{pp\pi}^{Pb-I}$	$t_{ss\sigma}^{Pb-Pb}$	$t_{sp\sigma}^{Pb-Pb}$	$t_{pp\sigma}^{Pb-Pb}$	$t_{pp\pi}^{Pb-Pb}$	λ
$\gamma = 1$	-7	2	-1.5	0.8	-1	1	-0.25	0.3	0.7	0.01	0.5
$\gamma = 0.74$	-7	2.5	-2	1	-1.2	1.5	-0.27	0.4	1.15	0.02	0.5

References

(1) Kore, A.; Kashikar, R.; Gupta, M.; Singh, P.; Nanda, B. Pressure and inversion symmetry breaking field-driven first-order phase transition and formation of Dirac circle in perovskites. *Phys. Rev. B* **2020**, *102*, 035116.

(2) Bhumla, P.; Kumar, M.; Bhattacharya, S. Theoretical insights into C–H bond activation of methane by transition metal clusters: the role of anharmonic effects. *Nanoscale Adv.* **2021**, *3*, 575–583.

(3) Bhattacharya, S.; Berger, D.; Reuter, K.; Ghiringhelli, L. M.; Levchenko, S. V. Theoretical evidence for unexpected O-rich phases at corners of MgO surfaces. *Phys. Rev. Mater.* **2017**, *1*, 071601.